INTERNATIONAL STUDIES IN THE FIELD OF

COMPUTER ENGINEERING

JUNE 2026

EDITOR
Prof. Dr. Selahattin BARDAK

gece kitaplığı

İmtiyaz Sahibi / Yaşar Hız
Yayına Hazırlayan / Gece Kitaplığı

Birinci Basım / Haziran 2026 - Ankara
ISBN / 978-625-321-139-4

Gece Kitaplığı
Kızılay Mah. Fevzi Çakmak 1. Sokak
Ümit Apt No: 22/A Çankaya/ANKARA
0312 384 80 40
www.gecekitapligi.com / gecekitapligi@gmail.com

Baskı & Cilt
Bizim Büro
Sertifika No: 42488

INTERNATIONAL STUDIES IN THE FIELD OF COMPUTER ENGINEERING

June 2026

EDITOR

Prof. Dr. Selahattin BARDAK

gece kitaplığı

CONTENTS

CHAPTER 1

MACHINE LEARNING FOR ENVIRONMENTAL SUSTAINABILITY: A METAHEURISTIC-OPTIMIZED EXTREME LEARNING MACHINE FOR CARBON EMISSION PREDICTION

Oluwatayomi Rereloluwa Adegboye 7

CHAPTER 2

MODELING OF HOT AIR DRYING KINETICS AND TEMPERATURE DISTRIBUTION IN WOOL YARN BOBBINS USING ANFIS

Uğur AKYOL, Halil Nusret BULUŞ, Soner ÇELEN 17

CHAPTER 3

A MULTI-STRATEGY ENHANCED ARTIFICIAL ELECTRIC FIELD ALGORITHM

Oluwatayomi Rereloluwa Adegboye 33

CHAPTER 1

MACHINE LEARNING FOR ENVIRONMENTAL SUSTAINABILITY: A METAHEURISTIC-OPTIMIZED EXTREME LEARNING MACHINE FOR CARBON EMISSION PREDICTION

Oluwatayomi Rereloluwa Adegboye [1]

1 Dr, University of Mediterranean Karpasia, 0000-0001-9945-8764, aoluwatayomi@gmail.com

Introduction

Artificial intelligence (AI) and machine learning (ML) have emerged as transformative tools for environmental sustainability, enabling data-driven insights that classical statistical models struggle to provide (Zennaro et al., 2021). Among the most pressing sustainability challenges is anthropogenic climate change, driven primarily by CO_2 emissions. The global mean temperature has risen 1.1°C above the 1850-1900 baseline (WMO Confirms 2024 as Warmest Year on Record at about 1.55°C above Pre-Industrial Level, 2025), threatening food security ('Climate Change Impacts on Global Food Security', n.d.) and public health ('CO2 Emission Sources, Greenhouse

Gases, and the Global Warming Effect', 2020). Accurate national-level CO_2 forecasting grounds mitigation pledges in evidence and supports carbon pricing.

ML-based emission models impose no linearity constraints and learn complex driver interactions, but face a recurring problem: random weight initialization produces run-to-run variance that undermines policy credibility. This chapter presents ELM-INFO - an ELM optimized by the INFO algorithm - as an interpretable case study in AI for sustainability.

Background

Machine Learning for Environmental Prediction

ML approaches to CO_2 forecasting span regression, ensemble methods, and deep learning (Bakay & Ağbulut, 2021; Hamrani et al., 2020; Mardani et al., 2020; Nguyen et al., 2021). A shared limitation across these approaches is that model architectures are selected. Hyperparameters are tuned manually, leaving internal parameters (weights, biases) to be set randomly - a design choice that introduces run-to-run variance and compounds with missing interpretability: most studies optimize prediction error but not driver attribution, which is the analysis policymakers need to prioritize interventions.

Extreme Learning Machine and Metaheuristic Optimization

ELM (Huang et al., 2004, 2006) trains SLFNs analytically via Moore-Penrose pseudoinverse, avoiding gradient-descent pitfalls (Wang et al., 2022), but is sensitive to random initialization. Population-based metaheuristics resolve this by searching the weight-bias space, and each has been paired with ELM, demonstrating consistent or accuracy gains over standalone ELM in structural, power, and battery engineering tasks (Shariati et al., 2022). A common limitation is reliance on single-strategy optimizers susceptible to premature convergence. INFO (Ahmadianfar et al., 2022) addresses this with a three-stage update (updating rule, vector combining, local search). The following section formalizes ELM, INFO, and their integration as the ELM-INFO framework that addresses both the initialization variance and interpretability gaps identified above (Feda et al., 2024).

Methodology

Extreme Learning Machine

ELM trains SLFNs with K hidden neurons by randomly assigning input weights w_j and biases b_j, then solving output weights analytically as given in Eq. (1).

$$f(\mathrm{x}) = \sum_{j=1}^{K} \beta_j G\left(\mathrm{w}_j^{\top}\mathrm{x} + b_j\right), \hat{\beta} = \mathrm{H}^{\dagger}\mathrm{T} \tag{1}$$

where $\mathrm{H} \in \mathbb{R}^{N\times K}$ is the hidden-layer output matrix and $G(\cdot)$ is an activation function. The closed-form solution eliminates iterative back-propagation but makes performance contingent on initialization quality (Wang et al., 2022).

INFO Algorithm

INFO (Ahmadianfar et al., 2022) operates on N_p candidates per generation g. Stage 1 (Updating Rule): weighted means of differentially selected vectors, modulated by wavelet functions and $\beta = 2e^{-4g/g_{\max}}$, promote diversity while accelerating convergence. Stage 2 (Vector Combining): stochastic merging ($\mu = 0.05 \cdot \mathrm{randn}$) intensifies exploitation near high-fitness regions. Stage 3 (Local Search): $\mathrm{x}_{\mathrm{md}} = \phi\mathrm{x}_{\mathrm{avg}} + (1-\phi)[\phi\mathrm{x}_{\mathrm{br}} + (1-\phi)\mathrm{x}_{\mathrm{bs}}]$ prevents local-optima entrapment; updates accepted greedily.

ELM-INFO Integration

Each INFO individual encodes a weight-bias candidate $(\mathrm{W}, \mathrm{b}) \in [-1,1]^D$, with fitness as described in Eq. (2)

$$\mathcal{F}(\mathrm{W}, \mathrm{b}) = \sqrt{\frac{1}{N}\sum_{i=1}^{N} \left(t_i - f(\mathrm{x}_i; \mathrm{W}, \mathrm{b})\right)^2} \tag{2}$$

After $g_{\max} = 200$ generations, the optimal $(\mathrm{W}^*, \mathrm{b}^*)$ initializes a final ELM trained analytically.

Empirical Application: Japan CO_2 Prediction

Dataset and Setup

The ELM-INFO model is applied to quarterly World Bank CO_2 data for Japan (1980-2021) (*World Bank Open Data*, n.d.). Four socioeconomic features - economic growth (EG), natural resources (NR), technological innovation (TI), and trade openness (TR) are min-max normalized. Training: 80%; testing: 20%; 10 -fold cross-validation. Baselines: ELM, ELM-GWO (Mirjalili et al., 2014), ELM-SSA (Mirjalili et al., 2017), ELM-SCA (Mirjalili, 2016); all with optimizer using population size of 30, and maximum iteration of 20, RMSE fitness.

Results and Feature Importance

Table 1 reports training and testing metrics. ELM-INFO achieves the best results on all five metrics in both phases: test R^2 of 0.974, RMSE of 0.19, demonstrating significant improvements over standalone ELM. The train-to-test R^2 gap is only $\Delta = 0.011$, confirming strong generalization.

Table 1: Training and testing performance metrics.

Model	Training					Testing				
	R^2	RMSE	MSE	MAE	MAPE	R^2	RMSE	MSE	MAE	MAPE
ELM	0.906	0.031	0.0010	0.025	0.014	0.906	0.037	0.0014	0.030	0.012
ELM-GWO	0.952	0.022	0.0005	0.017	0.009	0.959	0.025	0.0006	0.019	0.008
ELM-SSA	0.948	0.023	0.0005	0.017	0.009	0.959	0.024	0.0005	0.017	0.008
ELM-SCA	0.931	0.026	0.0007	0.020	0.010	0.946	0.028	0.0008	0.022	0.009
ELM-INFO	0.963	0.019	0.0003	0.014	0.006	0.974	0.019	0.0004	0.014	0.006

Permutation feature importance reveals that economic growth (EG) is the dominant driver in Fig. 1, directly linked to GDP-driven energy consumption and industrial CO_2 output in the dataset (Liu et al., 2023). Technological innovation is the second major driver in the model; the feature reflects the dual effect of technology on emissions: clean energy diffusion reduces them while fossil-fuel innovation can increase them (Zhao et al., 2023). Trade openness captures the pollution-haven effect and clean technology transfer channels. Natural resources have the smallest influence, consistent with Japan's manufacturing and service-driven economy.

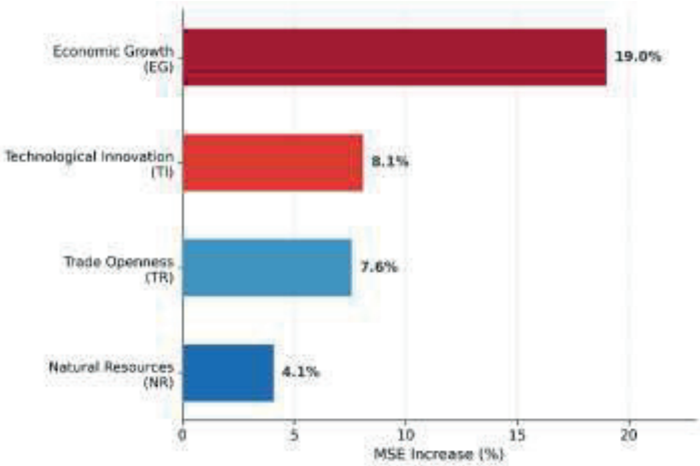

Figure 1. Feature Importance

Discussion

Implications for AI-Driven Sustainability Policy

ELM-INFO exemplifies how AI/ML can advance environmental sustainability not only through predictive accuracy but through interpretability: the permutation importance analysis translates a statistical model into actionable policy signals, bridging the gap between data science and governance. EG's dominance argues for growth-decoupled strategies carbon pricing, clean energy mandates, and industrial efficiency standards as the highest-leverage interventions for Japan's CO_2 reduction. TI's dual-direction effect implies that R&D subsidies should distinguish clean-energy from fossil-fuel technologies to avoid counterproductive emission effects. These findings illustrate a broader principle: ML-for-sustainability value is maximized when prediction and explanation are treated as co-equal objectives.

Conclusion

This chapter demonstrated ELM-INFO as a rhigh-accuracy tool for CO_2 emission prediction from socioeconomic data, contributing a practical case study to the AI/ML for environmental sustainability literature. On Japan's quarterly dataset, ELM-INFO achieves R^2 of 0.9742. Feature importance highlights economic growth as the primary policy lever for decarbonization. Future work should extend the framework to multi-country panels, incorporate temporal dynamics, and explore hybrid deep-metaheuristic architectures for long-range climate projection.

References

Ahmadianfar, I., Heidari, A. A., Noshadian, S., Chen, H., & Gandomi, A. H. (2022). INFO: An efficient optimization algorithm based on weighted mean of vectors. *Expert Systems with Applications*, *195*, 116516. https://doi.org/10.1016/j.eswa.2022.116516

Bakay, M. S., & Ağbulut, Ü. (2021). Electricity production based forecasting of greenhouse gas emissions in Turkey with deep learning, support vector machine and artificial neural network algorithms. *Journal of Cleaner Production*, *285*, 125324. https://doi.org/10.1016/j.jclepro.2020.125324

Climate Change Impacts on Global Food Security. (n.d.). *Science*. Retrieved 10 May 2026, from https://www.science.org/doi/10.1126/science.1239402

CO2 emission sources, greenhouse gases, and the global warming effect. (2020). In *Advances in Carbon Capture* (pp. 3–28). Woodhead Publishing. https://doi.org/10.1016/B978-0-12-819657-1.00001-3

Feda, A. K., Adegboye, O. R., Agyekum, E. B., Shuaibu Hassan, A., & Kamel, S. (2024). Carbon Emission Prediction Through the Harmonization of Extreme Learning Machine and INFO Algorithm. *IEEE Access*, *12*, 60310–60328. https://doi.org/10.1109/ACCESS.2024.3390408

Hamrani, A., Akbarzadeh, A., & Madramootoo, C. A. (2020). Machine learning for predicting greenhouse gas emissions from agricultural soils. *Science of The Total Environment*, *741*, 140338. https://doi.org/10.1016/j.scitotenv.2020.140338

Huang, G.-B., Zhu, Q.-Y., & Siew, C.-K. (2004). Extreme learning machine: A new learning scheme of feedforward neural networks. *2004 IEEE International Joint Conference on Neural Networks (IEEE Cat. No.04CH37541)*, *2*, 985–990 vol.2. https://doi.org/10.1109/IJCNN.2004.1380068

Huang, G.-B., Zhu, Q.-Y., & Siew, C.-K. (2006). Extreme learning machine: Theory and applications. *Neurocomputing, Neural Networks*, *70*(1), 489–501. https://doi.org/10.1016/j.neucom.2005.12.126

Liu, H., Wong, W.-K., The Cong, P., Nassani, A. A., Haffar, M., & Abu-Rumman, A. (2023). Linkage among Urbanization, energy Consumption, economic growth and carbon

Emissions. Panel data analysis for China using ARDL model. *Fuel*, *332*, 126122. https://doi.org/10.1016/j.fuel.2022.126122

Mardani, A., Liao, H., Nilashi, M., Alrasheedi, M., & Cavallaro, F. (2020). A multi-stage method to predict carbon dioxide emissions using dimensionality reduction, clustering, and machine learning techniques. *Journal of Cleaner Production*, *275*, 122942. https://doi.org/10.1016/j.jclepro.2020.122942

Mirjalili, S. (2016). SCA: A Sine Cosine Algorithm for solving optimization problems. *Knowledge-Based Systems*, *96*, 120–133. https://doi.org/10.1016/j.knosys.2015.12.022

Mirjalili, S., Gandomi, A. H., Mirjalili, S. Z., Saremi, S., Faris, H., & Mirjalili, S. M. (2017). Salp Swarm Algorithm: A bio-inspired optimizer for engineering design problems. *Advances in Engineering Software*, *114*, 163–191. https://doi.org/10.1016/j.advengsoft.2017.07.002

Mirjalili, S., Mirjalili, S. M., & Lewis, A. (2014). Grey Wolf Optimizer. *Advances in Engineering Software*, *69*, 46–61. https://doi.org/10.1016/j.advengsoft.2013.12.007

Nguyen, Q., Diaz-Rainey, I., & Kuruppuarachchi, D. (2021). Predicting corporate carbon footprints for climate finance risk analyses: A machine learning approach. *Energy Economics*, *95*, 105129. https://doi.org/10.1016/j.eneco.2021.105129

Shariati, M., Mafipour, M. S., Ghahremani, B., Azarhomayun, F., Ahmadi, M., Trung, N. T., & Shariati, A. (2022). A novel hybrid extreme learning machine–grey wolf optimizer (ELM-GWO) model to predict compressive strength of concrete with partial replacements for cement. *Engineering with Computers*, *38*(1), 757–779. https://doi.org/10.1007/s00366-020-01081-0

Wang, J., Lu, S., Wang, S.-H., & Zhang, Y.-D. (2022). A review on extreme learning machine. *Multimedia Tools and Applications*, *81*(29), 41611–41660. https://doi.org/10.1007/s11042-021-11007-7

WMO confirms 2024 as warmest year on record at about 1.55°C above pre-industrial level. (2025, January 10). World Meteorological Organization. https://wmo.int/news/media-centre/wmo-confirms-2024-warmest-year-record-about-155degc-above-pre-industrial-level

World Bank Open Data. (n.d.). World Bank Open Data. Retrieved 30 March 2024, from https://data.worldbank.org

Zennaro, F., Furlan, E., Simeoni, C., Torresan, S., Aslan, S., Critto, A., & Marcomini, A. (2021). Exploring machine learning potential for climate change risk assessment. *Earth-Science Reviews*, *220*, 103752. https://doi.org/10.1016/j.earscirev.2021.103752

Zhao, X., Xu, H., Yin, S., & Zhou, Y. (2023). Threshold effect of technological innovation on carbon emission intensity based on multi-source heterogeneous data. *Scientific Reports*, *13*(1), 19054. https://doi.org/10.1038/s41598-023-46406-3

CHAPTER 2

MODELING OF HOT AIR DRYING KINETICS AND TEMPERATURE DISTRIBUTION IN WOOL YARN BOBBINS USING ANFIS

Uğur AKYOL[1], Halil Nusret BULUŞ[2], Soner ÇELEN[3]

1 Prof.Dr. Tekirdağ Namık Kemal University, Çorlu Faculty of Engineering, Tekirdağ, ORCID ID: 0000-0003-3707-0929
2 Asist. Prof. Tekirdağ Namık Kemal University, Çorlu Faculty of Engineering, Tekirdağ, ORCID ID: 0000-0003-1844-6484
3 Prof.Dr. Tekirdağ Namık Kemal University, Çorlu Faculty of Engineering, Tekirdağ, ORCID ID: 0000-0001-5254-4411

INTRODUCTION

Drying is defined as the removal of liquid from a product's structure with the aid of thermal energy. In modern industry, it is widely utilized across numerous sectors, including textiles, food, paper, and pharmaceuticals. However, as with any industrial process, cost, quality, and efficiency remain the most critical challenges encountered in drying operations. Textile products are subjected to various finishing treatments during production phases; consequently, the moisture accumulated on the products during these stages is eliminated through drying, which constitutes the final step of the finishing process (Durak, 2012). A textile material can retain water equivalent to approximately 150% to 300% of its own weight (Akyol, 2007).

In the textile industry, products must undergo drying following dyeing and finishing treatments. The drying process is highly expensive and time-consuming, representing one of the highest cost components among textile finishing operations. Therefore, modeling the drying process by considering diverse drying conditions is of paramount importance (Durak, 2012). The term 'yarn' refers to a continuous strand derived by twisting textile fibers, filaments, or materials together (Houck and Siegel, 2015). Materials formed by winding yarns with a specific winding density onto perforated, hollow cylindrical, or conical carriers are termed yarn bobbins. Representative photographs of yarn bobbins are presented in Figure 1 (Karakoca, 2017).

Figure 1. Photographs of the yarn bobbins

In hot-air drying, thermal energy is transferred to the material via convection by passing heated air over the yarn bobbin, thereby enabling the removal of the evaporated liquid from the environment. This process continues until an equilibrium moisture content is established within the bobbin, depending on the temperature and moisture of the drying air (Toraman, 2011). The drying time and rate depend on the structural properties and surface area of the material, as well as the temperature, velocity, and moisture of the drying air. With the substantial increase in energy costs in recent years, determining the impact of these factors on the drying rate through mathematical models has gained paramount importance. This approach facilitates the design of optimum drying processes and the development of drying methodologies to minimize drying time without compromising the quality and structural integrity of the materials, while ensuring minimum energy consumption (Akyol, 2007).

In the spinning and weaving sectors, which are the fundamental components of the textile industry, the drying process represents one of the highest cost items among textile finishing operations. Systems in which drying is performed by passing hot air over the material surface are widely utilized in the textile industry (Toraman, 2011).

Throughout production in the textile industry, textile products are subjected to various finishing treatments, and the moisture absorbed during these processes is removed via drying. The essential objective in drying is to execute the process at minimum cost and in minimum time without damaging the hygroscopic structure of the textile product. In this work, the experimental drying behavior of the wool yarn bobbin was determined under different drying conditions. Utilizing the data obtained from convective drying experiments, the drying process was simulated using the ANFIS method. The obtained results were compared with both the experimental data and the empirical/semi-empirical mathematical models found in the literature. The results demonstrate that the values obtained through the artificial neural network method are in excellent agreement with the experimental data.

Experimental Apparatus and Procedure

Hot air drying operations of wool yarn bobbins were carried out utilizing the experimental apparatus located at Tekirdağ Namık Kemal University. Wool yarns of various counts, widely preferred in the Turkish textile industry, were employed as the raw material. The test specimens comprised a blend of 65% wool and 35% orlon. Due to the induced pressure difference, the heated air was forced solely through the interior of the bobbins, establishing an inside-to-outside drying front. The experimental trials were performed under a hot air flow rate of 450 m^3/h, a temperature of 90 °C, and gauge pressures of 1, 2, and 3 bar. The dimensions of the yarn bobbins were characterized by an internal diameter of 35 mm and a total length of 150 mm. To enable efficient air transport, the yarn was wound onto a perforated tube manufactured from high-density polyethylene

(a) (b) (c)

Figure 2 Material and setup, a) Spool b) Yarn bobbin, c) Drying chamber

Prior to the drying process, the bobbins were immersed in a water bath for 12 h. Following the water bath, the bobbins were placed on a grid for 30 min to drain excess surface water and ensure uniform moisture penetration into the yarn fibers. After draining, the bobbins underwent a pre-drying phase with cold air (without engaging the heating elements) for approximately 10 min to remove a portion of the residual excess water. Subsequently, the actual drying process was executed under the predefined system conditions. The yarn bobbins exhibited an initial conditioned mass of around 8.27±0.05 g, which decreased to a final equilibrium mass of approximately 5.00±0.05 g.

As illustrated in Figure 3, thermocouples were positioned at equal intervals and at different angles. Experimental observations indicated that the temperature did not vary significantly along the length of the bobbin. Consequently, only the variations in the radial directions were taken into consideration during the development of the mathematical model.

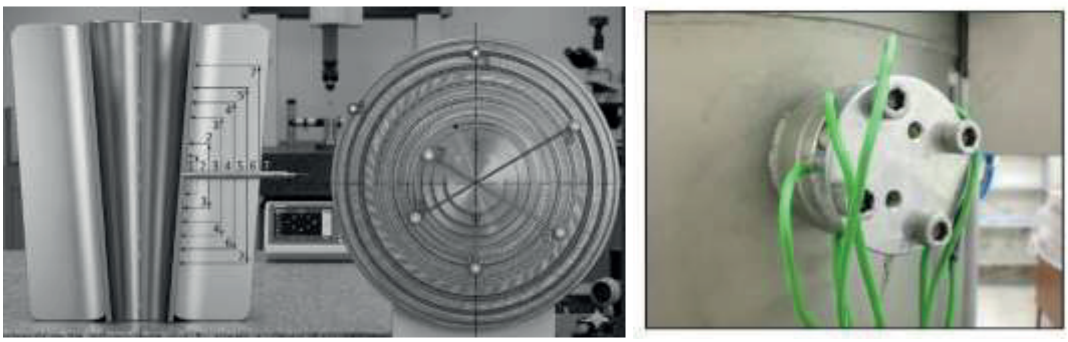

Figure 3. Temperature measurement points locations within the yarn bobbin

Throughout the drying operation, multiple thermal zones—including the inlet (IT) and outlet (OT) of the chamber, the inner chamber environment (CIT), the separator (ST), and the fan exhaust (FOT)—were monitored via thermocouples. The acquired measurements were subsequently transmitted to a digital platform. Ultimately, a forecasting analysis was conducted to estimate these five measured temperature values.

Moisture ratio of the yarn bobbin

The wet-basis moisture content of the yarn bobbin sample was evaluated via Equation 1. The moisture ratio (MR) was subsequently established by calculating the ratio between the moisture content (MC) at any specific time t and its initial state (M_0) according to Equation 2 (Çelen and Karataşer, 2019). Here, the variables M and M_d represent the dynamic mass of the product during the process and its final dried mass, respectively.

$$MC_{wb}(\%) = (\frac{M-M_d}{M})\times 100 \tag{1}$$

$$MR = \frac{MC-M_e}{M_o-M_e} \tag{2}$$

Adaptive Neuro-Fuzzy Inference System (ANFIS)

ANFIS synthesizes the adaptive self-learning capability of artificial neural networks with the linguistic expression features of fuzzy logic. In order to optimize the parameters of a Takagi-Sugeno fuzzy inference system, ANFIS employs a hybrid learning algorithm that couples least-squares estimation with the backpropagation gradient method. Structurally, ANFIS operates as a multilayered feedforward network where each node performs a designated operation on signals based on its own parameter set. Through extracting underlying rules from historical datasets, ANFIS is capable of mapping novel inputs onto accurate output profiles. The schematic architecture of ANFIS is depicted.

The architecture of the ANFIS model is characterized by five separate layers, where each layer encompasses nodes characterized by distinct node functions. Layer 1 is composed of adaptive nodes, each possessing a dedicated node function. Layer 2 is the rule layer, where the node multiplies incoming signals, meaning the resulting output is the product of all incoming vectors.

Layer 3 normalizes the firing strengths by calculating the ratio of the i-th rule's firing intensity to the total firing strength of all rules. In Layer 4, every node determines the consequent parameters and evaluates the i-th rule's contribution to the global output. In Layer 5, the single output node aggregates all incoming signals to compute the overall final output.The ANFIS modeling framework comprises three primary phases: training, validation (checking), and testing. The allocation of the dataset employed across these steps is summarized in Table 1.

Table 1. Categorization of Data in Modeling

Category	Percentage	Number of Specimens
Tarining & Validation	80%	1229
Test	20%	307
Total	100%	1536

In the fuzzy approach, the consequent part of a rule is inherently a linguistic expression provided by an expert. However, through the Sugeno method (Jang, 1993), this linguistic information is mathematically formulated as a function of the linear combination of inputs, as expressed in Equations 5 and 6.

Rule 1: If $x = A_1$ and $y = B_1$, then $f_1 = p_1x + q_1y + r_1$ (3)

Rule 2: If $x = A_2$ and $y = B_2$, then $f_2 = p_2x + q_2y + r_2$ (4)

Here, x and y represent the input variables. A denotes the fuzzified value determined by the membership function employed in the fuzzification layer. The terms p, q, and r define the parameter set of the respective rule. Consequently, f_i signifies the output derived from that specific rule. The final global output is calculated as the weighted average of all rules, as formulated in Equation 5 (Singpurwalla and Booker, 2004):

$$f = \frac{w_1 f_1 + w_2 f_2}{w_1 + w_2} \quad (5)$$

where f is the final output obtained utilizing the weights and input data, and w represents the firing strength (weight) determined by the inference system. In scenarios where inputs and outputs are predefined, the weight values (w) are optimized by the ANFIS network through ANN learning algorithms, enabling the system to model datasets with unknown outcomes.

The ANFIS architecture comprises five layers. In this study, a total of 9 variables—consisting of 7 inputs and 2 outputs—were utilized within the ANFIS framework. In the first layer, these input values are mapped to their respective degrees of membership via a membership function. In the second layer, the inputs are multiplied at each node to generate the rule's firing strength. In the third layer, the firing strengths are normalized by calculating the ratio of individual rule strengths to the total firing strength. Following the third layer, the Sugeno fuzzy model is executed in the fourth layer. Finally, the fifth layer aggregates all incoming signals to yield the total final output. Since the ANFIS tool in the MATLAB platform does not accommodate multiple outputs, two distinct ANFIS models were developed to predict moisture ratio (MR) and mass independently. Identical training and testing datasets were employed for both models, each generating 27 fuzzy rules. The simulation was executed in MATLAB software using the ANFIS toolbox.

Statistical analysis

The optimization of the system modeling was achieved through the implementation of various artificial intelligence techniques. Evaluation of the model’s performance relied on identifying the output that minimized prediction discrepancies, as verified by several performance metrics including the coefficient of determination (R^2), MAPE, RMSE, and MAE (Eqs. 6–9) (Buluş et al., 2024).

$$\mathrm{R}^2 = 1 - \left[\frac{\sum_{\mathrm{i}=1}^{\mathrm{N}}\left(MR_{\mathrm{pre,i}} - MR_{\mathrm{exp,i}}\right)^2}{\sum_{\mathrm{i}=1}^{\mathrm{N}}\left(MR_{\mathrm{pre,i}} - MR_{exp,i}\right)^2}\right] \tag{6}$$

$$\mathrm{MSE} = \left[\frac{1}{\mathrm{n}}\sum_{\mathrm{i}=1}^{\mathrm{n}}\left(MR_{\mathrm{pre,i}} - MR_{\mathrm{exp,i}}\right)^2\right] \tag{7}$$

$$\mathrm{RMSE} = \left[\frac{1}{\mathrm{n}}\sum_{\mathrm{i}=1}^{\mathrm{n}}\left(MR_{\mathrm{pre,i}} - MR_{\mathrm{exp,i}}\right)^2\right]^{1/2} \tag{8}$$

$$\mathrm{MAPE} = \frac{1}{\mathrm{n}}\left[100 \times \frac{MR_{\mathrm{exp,i}} - MR_{\mathrm{pre,i}}}{MR_{\mathrm{exp,i}}}\right] \tag{9}$$

These metrics are standard in machine learning applications for regression analysis. In this study, MATLAB was utilized to perform regression analysis and estimate model parameters.

The performance of the developed ANFIS models was assessed based on R^2, RMSE, and MAPE values. The model with the highest R^2, lowest RMSE, and MAPE under 10% was deemed the most effective in predicting experimental moisture content and drying rate with respect to drying time, consistent with prior research (Moralar, 2024; Buluş, 2024).

A one-way analysis of variance (ANOVA) was conducted to examine the influence of temperature (90 °C) and pressure levels (1–3 bar) on the moisture ratio (MR) and sample mass (M). Subsequently, the Least Significant Difference (LSD) post-hoc test was applied to determine whether the observed differences were statistically significant.

RESULTS AND DISCUSSION

By inherent design, the standard ANFIS structure is built upon a single output (MISO - Multiple Input Single Output). In this study, however, we deal with two distinct outputs: Chamber Outlet Moisture and Separator Outlet Moisture. To address this challenge, two separate ANFIS models were constructed and trained, thereby yielding independent results for each output. During the data preparation phase, incorporating the moisture value from the previous time step (t-1)—alongside instantaneous inputs such as the coil drying value, pressure, and temperature—substantially enhances the predictive capability of the model.

Furthermore, a Takagi-Sugeno type ANFIS architecture was employed in this study to effectively model the non-linear and time-dependent dynamics of the industrial drying process. Compared to traditional Mamdani fuzzy inference systems, the Takagi-Sugeno framework offers superior computational speed due to its use of mathematical functions (linear equations) in the consequent layer. Additionally, it provides robust hybrid learning capability that combines the Least Squares Estimator (LSE) with Gradient Descent for parameter optimization. This approach not only enhances model stability but also facilitates integration into real-time industrial control applications and enables the generation of an interpretable rule base.

In time-series and industrial process data, applying random shuffling leads to data leakage, causing the model to artificially "memorize" future data based on past observations. Consequently, the dataset must be partitioned chronologically. In this study, the time-series dataset of the industrial drying process was split chronologically (sequentially) to preserve temporal dependencies and prevent data leakage. Specifically, 80% of the total dataset was allocated for model training and internal validation (tuning gradient descent parameters during the hybrid learning process), while the remaining 20% was reserved for testing to evaluate the model's ultimate generalization capability on entirely unseen data.

Table 2. Data Distribution Table

Dataset Block	Ratio (%)	Purpose of Utilization	Methodology
Training & Validation (Train / Val)	80%	Training of ANFIS consequent parameters (LSE) and membership function parameters (Gradient Descent).	The first 80% chronological data block.
Test (Test Set)	20%	Evaluation of the trained ANFIS model's real-time prediction performance and calculation of RMSE and related metrics.	The final 20% chronological data block.

The models based on the ratios provided in the Table 2 constitute the 5-layer architecture, as illustrated in Figure 4.

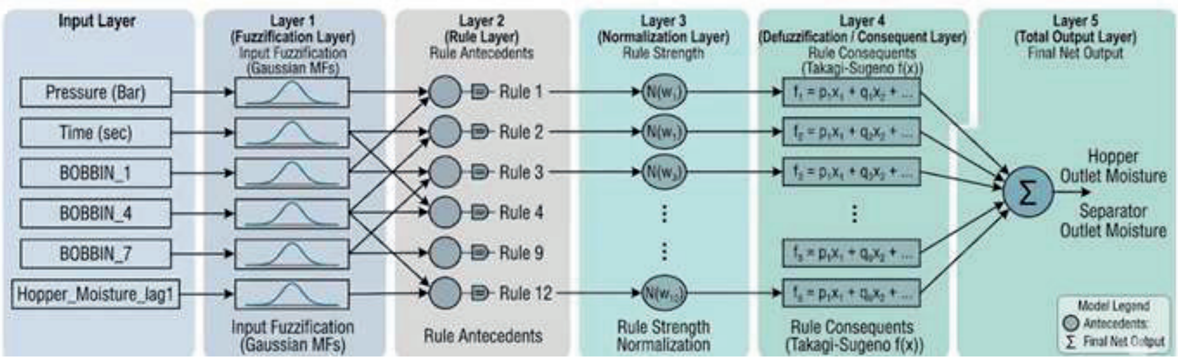

Figure 4. Demonstration Of Anfis Architecture And Performance Metrics

The fields provided as inputs to the models were determined as pressure, time, and 7 coil temperature values. The R^2 and RMSE values obtained from the baseline ANFIS models configuration using these specified inputs are presented in Table 3 and Figure 5.

Table 3. Baseline ANFIS Model Performance Metrics

Output	R^2	RMSE
Hopper Outlet Moisture	-1.6799	59.6030
Separator Outlet Moisture	-3.5661	14.1434

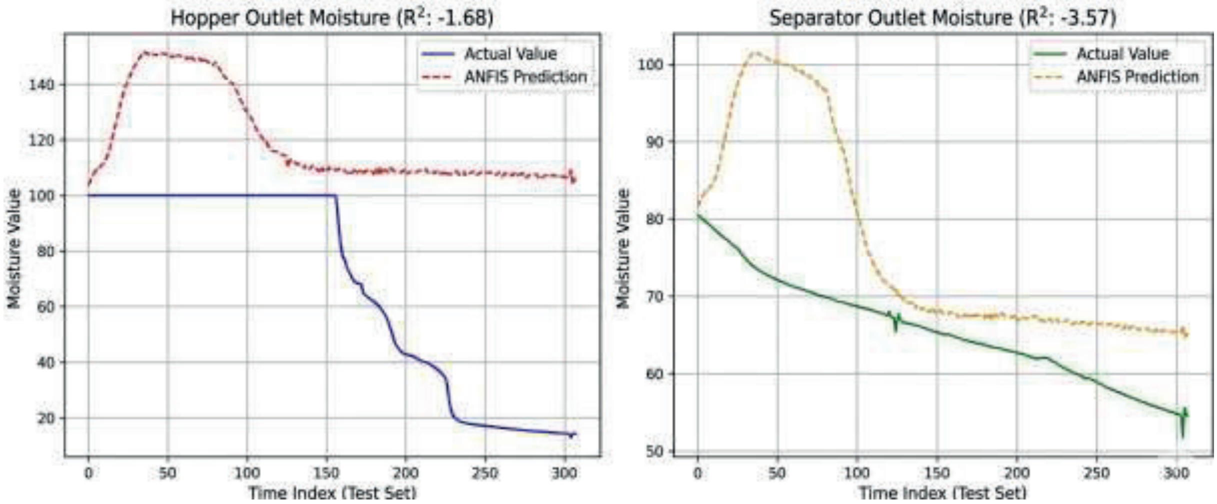

Figure 5. Performance Evaluation of the Baseline ANFIS Model for Moisture Prediction

When the performance metrics are examined, it is evident that the baseline model generates unsuccessful predictions. The negative R^2 values and high RMSE scores clearly indicate that the model has not yet captured the underlying dynamics of the dataset.

This sub-optimal performance can be attributed to the following factors:

- **Time-Lag Effect:** The drying and moisture processes inherently operate with a time lag; however, these lagged variables were not incorporated into the model as inputs.
- **Insufficient Model Complexity and Underfitting:** Employing only 4 rules (n_rules = 4) for 8 inputs and training for a mere 30 epochs may have rendered the model architecture too weak to resolve the complex physical nature of the process.
- **Mathematical Instability:** When the variance (variability) in the output is critically low, mathematical models—specifically matrix inversion operations during the Least Squares Estimation (LSE) phase—tend to become unstable, leading to invalid predictions.

Based on the aforementioned limitations, the following adjustments are proposed to enhance the performance of the ANFIS models:

Integration of Lagged Features: The values of each coil and pressure data from the previous time step (t-1) will be included in the input vector.

Expansion of the Rule Base: The number of fuzzy rules will be increased to improve the learning capacity of the model.

Prolonged Training Duration: The training duration (number of epochs) will be extended to ensure proper convergence.

The R^2 and RMSE values obtained from the baseline ANFIS models configuration using these specified inputs are presented in Table 4 and Figure 6.

Table 4. Baseline ANFIS Model Performance Metrics

Output	R^2	RMSE
Hopper Outlet Moisture	-7.2509	104.6157
Separator Outlet Moisture	-0.1637	7.0922

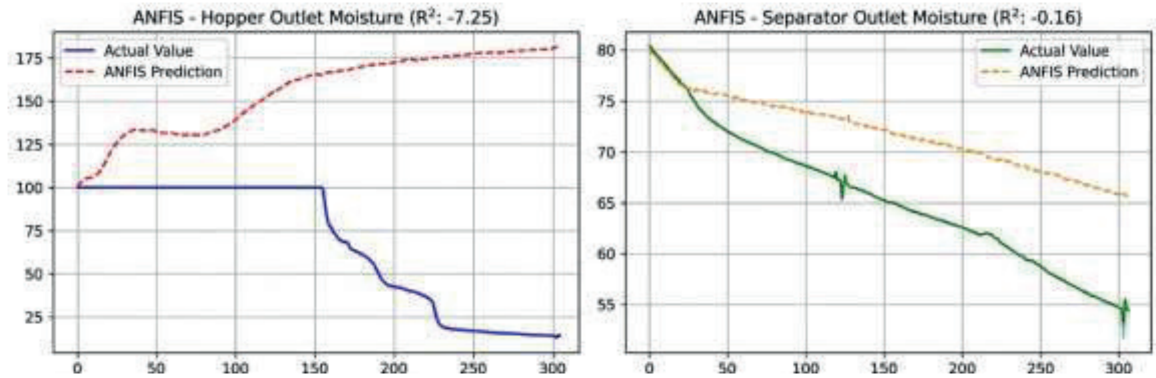

Figure 6. Comparison of ANFIS model predictions against actual values for hopper and separator outlet moisture, including model performance metrics.

The obtained values did not provide a positive contribution to improving the prediction performance. This sub-optimal outcome can be attributed to the "Curse of Dimensionality" (Rule Explosion), which represents the most significant limitation of the ANFIS architecture. Since the time lags of the last two steps were incorporated into the model, a total of 27 inputs were generated. Consequently, when utilizing 6 fuzzy rules, the underlying Least Squares Estimation (LSE) matrix of the ANFIS model expands to an overwhelming magnitude.

To resolve this limitation, a feature importance analysis was conducted to identify the most critical input variables (Figure 7). The selected key features are determined as: Bar, Time, Bobbin1, Bobbin 4, and Bobbin 7. Furthermore, only a single time-lag step (t-1) of these specific inputs was integrated into the model. By mitigating the dimensionality of the input space, it is intended to enable the ANFIS model to generate significantly more precise and well-defined decision-making boundaries.

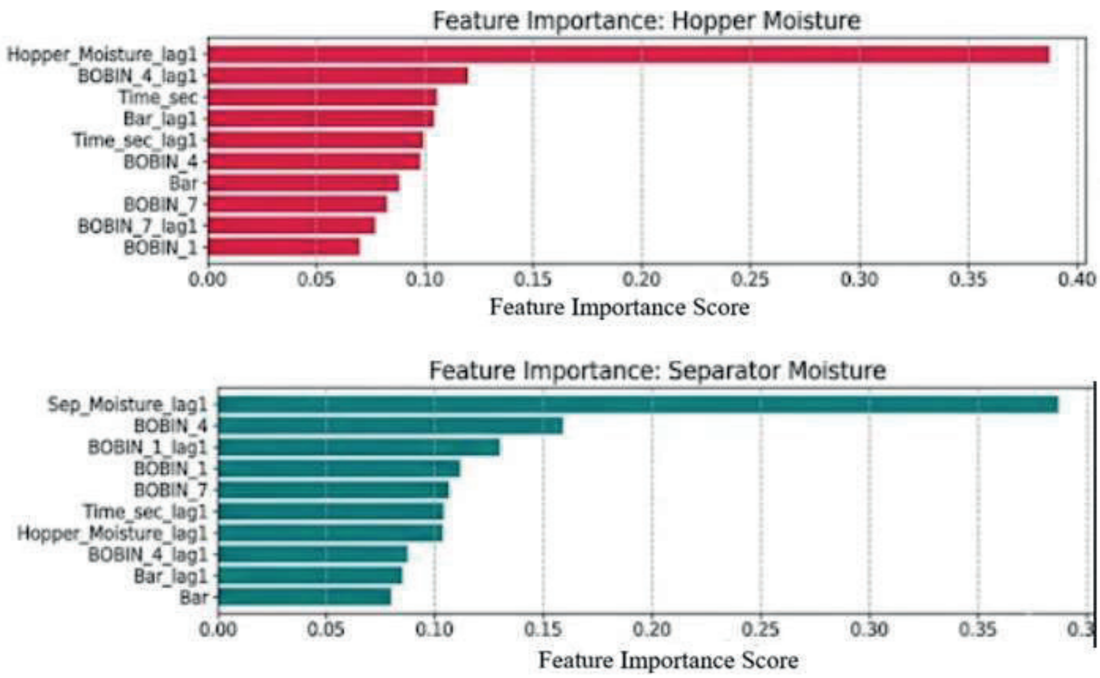

Figure 7. Feature Importance Analysis for Input Variables in the ANFIS Models

Furthermore, during drying processes, the self-lagged value of the hopper or separator moisture from 10 seconds prior (t-1) carries a significantly stronger predictive signal compared to the coil temperatures. Consequently, the Hopper Moisture lag1 and Sep Moisture lag1 features were directly fed into the ANFIS model as primary inputs.

Regarding the optimization phase, maintaining a constant learning rate (lr) of lr = 0.01 during Gradient Descent may cause the model to overshoot the optimum point and oscillate around it while updating the centers (means) of the membership functions. To mitigate this issue, a learning rate decay mechanism (lr = lr× 0.95) that dynamically decreases the learning rate as the training progresses has been integrated into the architecture.

Additionally, to enhance the overall architectural flexibility of the system, it is planned to scale the rule base from 6 to a more adaptable structure of 12 rufles, alongside further optimizing the initial spread (sigma) parameters of the Gaussian membership functions.

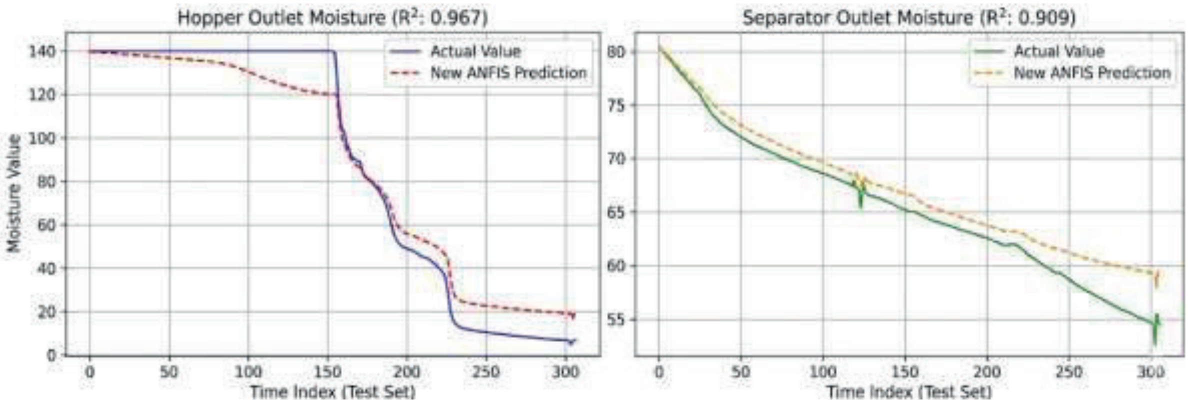

Figure 8. Time-series validation curves of the refined ANFIS predictor

The R^2 scores, as key performance metrics, were calculated as 0.9667 and 0.9086 for the hopper outlet moisture and separator outlet moisture, respectively (Figure 8). Supplementing these successful predictions, the remaining performance evaluation metrics were also computed and are presented in Table 5.

Table 5. Performance Metrics of the Optimized ANFIS Model over the Test Dataset

Output	R^2	RMSE	MAE	MAPE (%)
Hopper Outlet Moisture	0.9667	6.6492	5.5460	18.6093
Separator Outlet Moisture	0.9086	1.9873	1.6258	2.6591

A negative coefficient of determination (R^2) demonstrates that the model fails to capture the underlying relationship between the inputs and outputs, performing worse than a simple horizontal predictor based on the historical mean of the data. The primary reason for this sub-optimal performance can be attributed to the fact that instantaneous data points fail to capture the thermal and physical propagation delays (thermal lag) inherent in drying ovens. Furthermore, introducing an excessive number of coil parameters triggered a "rule explosion," which subsequently overwhelmed the Least Squares Estimation (LSE) linear solver layer of the ANFIS architecture.

Through systematic feature engineering and an "evolved ANFIS" approach, the input space was downscaled to the three most critical coil parameters, and temporal memory was integrated into the system by introducing lag-1 (t-1) variables. Following this reconfiguration, the model generated values that closely align with the targeted outcomes.

The achieved R^2 scores (0.9667 and 0.9086) indicate that the proposed model successfully accounts for 96.67% of the variance and fluctuation in the hopper outlet moisture. The RMSE values (6.6492 and 1.9873) alongside the MAE metrics (5.5460 and 1.6258) reveal that the overall mean prediction errors hover around 5.54 and 1.63 units, respectively. The proximity of the RMSE values to the MAE metrics further substantiates that the test dataset is free from severe outliers that would otherwise cause major model deviations.

Given the highly volatile nature of industrial drying processes, the MAPE value for the hopper (18.6093%) is considered to be within acceptable industrial tolerances. Concurrently, the exceptionally low absolute percentage error observed in the separator outlet moisture prediction (2.6591%) stands out as a highly precise result.

In conclusion, the matrix instabilities and negative R^2 phenomena encountered in the initial ANFIS designs were completely resolved by optimizing the fuzzy rule base and integrating autoregressive time-lagged variables (t-1). The finalized Takagi-Sugeno ANFIS models demonstrated superior generalization capability and numerical stability over the test dataset for both the Hopper (R^2 = 0.9667) and the Separator (R^2 = 0.9086, MAPE = 2.65%).

CONCLUSIONS

In this study, an ANFIS framework was optimized to predict the transient moisture dynamics of wool yarn bobbins in an industrial drying process. While the initial baseline ANFIS models suffered from severe numerical instability and negative determination coefficients (R^2 = -1.68 for the hopper and R^2= -3.57 for the separator) due to the curse of dimensionality and unmodeled thermal lag, systematic feature engineering effectively resolved these limitations.

By utilizing feature importance scores, the input space was downscaled to the most critical variables, and temporal memory was integrated into the network via autoregressive time-lagged parameters (t-1). Furthermore, a learning rate decay mechanism (lr= lr×0.95) was implemented to eliminate localized numerical oscillations.

The finalized Takagi-Sugeno ANFIS model demonstrated robust generalization capability and high prediction accuracy over the independent test dataset:

- **Hopper Outlet Moisture Prediction:** Achieved an R^2 score of 0.9667, an RMSE of 6.6492, and an MAE of 5.5460, demonstrating that the model accounts for 96.67% of the transient variance.
- **Separator Outlet Moisture Prediction:** Yielded an outstanding R^2 score of 0.9086, an RMSE of 1.9873, and a remarkably low MAPE of 2.6591%.

The strong proximity between the RMSE and MAE values confirms the absence of severe outlier prediction errors, validating the reliability of the network architecture. In conclusion, the proposed optimized ANFIS model provides a powerful, computationally stable, and highly accurate alternative for real-time moisture monitoring and control in industrial textile drying operations. Future work will focus on integrating this soft-computing predictor into programmable logic controllers (PLCs) for adaptive energy-saving process control.

REFERENCES

Akyol, U., (2007). Theoretical investigation for drying of yarn bobbins, Trakya University Institute of Natural and Applied Sciences, PhD, edirne, Türkiye.

Buluş, H.N. (2024). Adaptive Neuro-Fuzzy Inference System and Artificial Neural Network Models for Predicting Time-Dependent Moisture Levels in Hazelnut Shells (*Corylus avellana L.*) and Prina (*Oleae europapeae L.*), *Processes*, 12(8), 1703. https://doi.org/10.3390/pr12081703

Buluş, H.N., Akyol, U., Subaşı, N. & Çelen, S. (2024). Predictıon of the internal temperatures of the yarn bobbin during, Drying**,** Iksad publishing, Ed:Bellitürk, K., 243-267.

Çelen, S., & Karataşer, M. A. (2019). Investigation of the performance of a hybrid dryer designed for the food industry, *Foods,* 8(2), 81. https://doi.org/10.3390/foods8020081.

Durak, A. (2012). Modeling of a convective drying process by using artificial neural networks method, MsC. Thesis, Namık Kemal University, Tekirdağ, Türkiye.

Houck, M.M., & Siegel, J.A. (2015). *Fundamentals of Forensic Science* (3rd Edition). Oxford, 703s, İngiltere.

Jang, J.S.R. (1993) ANFIS: Adaptive-network-based fuzzy inference system. *IEEE Transactions on Systems Man & Cybernetics*, 23, 665-685.

Karakoca, A. (2017). Determination of temperature field for drying process of yarn bobbins using finite difference method, MsC. Thesis, Namık Kemal University, Tekirdağ, Türkiye.

Moralar, A. (2024). Modeling drying process parameters for petroleum drilling sludge with ANN and ANFIS, *Processes*, 12(9), 1948. https://doi.org/10.3390/pr12091948.

Singpurwalla, N. D., & Booker, J. M. (2004). Membership functions and probability measures of fuzzy sets. *Journal Of The American Statistical Association*, 99(467), 867-877. doi:10.1198/016214504000001196.

Toraman, S. (2011). Experimental ınvestigation of drying behavior of wool bobbins, MsC. Thesis, Namık Kemal University, Tekirdağ, Türkiye.

CHAPTER 3

A MULTI-STRATEGY ENHANCED ARTIFICIAL ELECTRIC FIELD ALGORITHM

Oluwatayomi Rereloluwa Adegboye [1]

1 Dr, University of Mediterranean Karpasia, 0000-0001-9945-8764, aoluwatayomi@gmail.com

Introduction

Metaheuristic optimization algorithms have become essential tools for solving derivative-free, black-box optimization problems arising in engineering design, parameter estimation, and computing (Singh & Kumar, 2021; Wolpert & Macready, 1997; Yang, 2010). Unlike gradient-based methods, metaheuristics impose no differentiability requirements and can navigate rugged, discontinuous, and multimodal objective landscapes by coordinating a population of candidate solutions through stochastic operators that mimic natural or physical phenomena (Kennedy & Eberhart, 1995; Rashedi et al., 2009). This generality has driven the development of a rich family of swarm intelligence and evolutionary computation methods, including Particle Swarm Optimization (PSO) (Kennedy & Eberhart, 1995), Differential Evolution (DE) (Storn & Price, 1997), Sine Cosine Algorithm (SCA) (Mirjalili, 2016), JAYA (Venkata Rao, 2016), and Cuckoo Search (CS) (Yang & Deb, 2010). Among physics-inspired approaches, the Artificial Electric Field Algorithm (AEFA) (Anita & Yadav, 2019) models each particle as an electrically charged agent whose trajectory is governed by Coulomb's law of electrostatic attraction toward higher-quality regions of the search space. AEFA has demonstrated competitive convergence speed on classical benchmark functions; however, it shares a fundamental limitation with many attraction-based physics-inspired algorithms: as the swarm evolves, Coulomb forces progressively draw all particles toward a single dominant agent, causing rapid population homogenization. This premature convergence prevents the algorithm from exploring alternative basins of attraction and leads to entrapment in local optima, a failure mode that is exacerbated at higher problem dimensions and on multimodal landscapes.

Two complementary strategies have been shown to mitigate premature convergence in population-based optimizers. First, opposition-based initialization strategies (Rahnamayan et al., 2008) (Khishe, 2023) create the initial population with both candidate solutions and their opposite counterparts, expanding the effective search landscape from the very first generation. Specular Reflection Learning (SRL) (Zhang, 2021) generalizes this principle by reflecting each initial particle across the midpoint of the search domain with a tunable coefficient, enabling broader and more flexible initial coverage than strict opposition. Second, local escaping operators embedded within the position-update step allow individual agents to escape basins of attraction during search. The Local Escaping Operator (LEO) introduced in the Gradient Based Optimizer (Ahmadianfar et al., 2020) achieves this by constructing alternative positions through arithmetic combinations of the global best, two random probe points, and random population members, governed by a nonlinear schedule that decays from exploration to exploitation over iterations.

This paper presents GSLEO-AEFA (Adegboye & Deniz Ülker, 2023), a novel enhanced variant of AEFA that integrates three mutually reinforcing mechanisms to address all identified failure modes simultaneously. The contributions of this work are as follows:

- The standard random initialization of AEFA is replaced by SRL, which generates each initial particle's specular reflection across the search domain. Gaussian Mutation (GM) is then applied to each reflected candidate to disrupt residual population symmetry, yielding a diverse initial swarm with broad spatial coverage.
- LEO integration into position updates: At each iteration, an agent's next position is computed via the LEO formula rather than the standard AEFA velocity update, providing a structured mechanism for escaping local optima throughout the search without disrupting the charge-based dynamics.

Related Work

Physics-Inspired Optimization Algorithms

Physics-inspired metaheuristics exploit fundamental principles from classical mechanics, electrostatics, and molecular dynamics to define inter-agent interaction rules that emerge into effective global search behavior. The Gravitational Search Algorithm (GSA) (Rashedi et al., 2009) models each agent as a mass that exerts and responds to gravitational attractions; heavier (fitter) masses attract lighter masses across the entire population, producing a convergence mechanism structurally analogous to the Coulomb force model of AEFA (Anita & Yadav, 2019). The Charged System Search (CSS) (Kaveh & Talatahari, 2010) models particles as electrically charged spheres subject to Coulomb and Gauss laws, accelerating toward stronger charges based on fitness-derived charge magnitudes. These methods share a decisive advantage: they are parameter lean and exhibit rapid exploitation of high-quality regions identified early in the search.

A known weakness of attraction-force frameworks, including AEFA, GSA, and CSS, is population homogenization. As fit agents accumulate a disproportionate share of the charge or mass, the inter-agent forces pull the entire swarm toward a single attractor. The resulting loss of diversity prevents the population from sampling distant search regions and renders the algorithm vulnerable to entrapment in local optima, particularly on high-dimensional multimodal problems. Subsequent physics-inspired methods, such as Harris Hawks Optimization (HHO) (Heidari et al., 2019) and the Grey Wolf Optimizer (GWO) (Mirjalili et al., 2014), partially mitigate this issue by incorporating multiple attractors (alpha, beta, and delta in GWO; multiple phase transitions in HHO). The present work addresses the homogenization problem through enhanced initialization and a dedicated position-perturbation operator embedded within the AEFA update cycle.

Diversity Enhancement and Local Search Hybridization

Opposition-Based Learning (OBL) doubles effective initialization coverage by simultaneously evaluating each candidate and its complement $x^* = lb + ub - x$. Rahnamayan et al. (Rahnamayan et al., 2008) demonstrated substantially faster convergence when OBL was integrated into Differential Evolution. Specular Reflection Learning (SRL) (Zhang, 2021) generalizes OBL with a tunable coefficient samples the intermediate region, avoiding the symmetry of exact opposite reflection. Gaussian Mutation (GM) further disrupts residual symmetry by applying a zero-mean Gaussian perturbation to each reflected individual, retaining the mutated point only if it improves on its parent.

Hybrid metaheuristics that embed local refinement within global search are well-established (Neri & Cotta, 2012). The Local Escaping Operator (LEO) (Ahmadianfar et al., 2020) from the Gradient-Based Optimizer constructs two alternative positions per iteration - one anchored to the current particle, one to the global best - perturbed by random probe points and population members. A sinusoidally decaying factor transitions LEO from broad exploration to fine exploitation. The Slime Mould Algorithm (SMA) (Li et al., 2020) and Krill Herd (Gandomi & Alavi, 2012) employ analogous adaptive mechanisms. The present work embeds LEO directly in the AEFA position update cycle, activating with probability 0.5 per particle per iteration, preserving charge-based dynamics while providing a structured local escape path.

Proposed Method

Specular Reflection Learning with Gaussian Mutation

Random initialization provides no prior information about the search space, increasing the probability that the initial swarm concentrates near one region and misses distant optima. SRL addresses this by reflecting each initial candidate $p_i \in [p_{\min}, p_{\max}]^D$ across the domain midpoint as defined in Eq. (1)

$$p^* = (0.5\mu + 0.5)(p_{\min} + p_{\max}) - \mu p_i \tag{1}$$

where $\mu \in [0,1]$ is a scaling factor that controls the reflection distance. Setting $\mu = 1$ recovers standard OBL; values $\mu < 1$ produce reflections that lie between p_i and its OBL opposite, sampling the intermediate region. To eliminate residual symmetry introduced by any deterministic reflection, Gaussian Mutation is applied to each reflected individual Eq. (2)

$$p_{g,i} = p^* \cdot (1 + \gamma \mathcal{N}(0,1)) \tag{2}$$

where γ governs the perturbation magnitude. The mutated individual $p_{g,i}$ is accepted if it improves on p^*; otherwise p^* is retained. After evaluating both the original population and the SRL and GM population, the N fittest individuals across both sets form the initial swarm, combining broad spatial coverage with elitist selection.

Local Escaping Operator

The LEO, adapted from GBO, is applied at each iteration to provide a gradient-free escape mechanism. Let P_n^m denote the m-th dimension of particle n 's current position, P_{best} the global best, and P_{r1}^m, P_{r2}^m two randomly selected population members. Two random probe positions $P1_n^m, P2_n^m \sim \mathcal{U}(lb, ub)$ are generated. With probability 0.5, the update is expressed in Eqs. (3) and (4)

$$P_{\text{LEO}} = P_n^m + f_1(u_1 P_{\text{best}} - u_2 P_k^m) + f_2 \rho_1 \big(u_3 (P2_n^m - P1_n^m)\big) + \frac{u_2}{2}(P_{r1}^m - P_{r2}^m)/2 \tag{3}$$

Otherwise, it centers on the global best:

$$P_{\text{LEO}} = P_{\text{best}} + f_1(u_1 P_{\text{best}} - u_2 P_k^m) + f_2 \rho_1 \big(u_3 (P2_n^m - P1_n^m)\big) + \frac{u_2}{2}(P_{r1}^m = P_{r2}^m)/2 \tag{4}$$

Here $f_1, f_2 \sim \mathcal{U}(-1,1)$, and u_1, u_2, u_3 are binary-modulated random scalars defined as $u_j = L_1 \cdot r_j + (1 - L_1)$, where $r_j \sim \mathcal{U}(0,1)$ and $L_1 = 1[k_1 < 0.5]$ with $k_1 \sim \mathcal{U}(0,1)$. The probe term P_k^m is either a uniformly random position or a random population member, selected with equal probability. The nonlinear factor $\rho_1 = 2r\alpha - \alpha$ decays via Eq. (5)

$$\alpha = \left|\beta \sin\left(\frac{3\pi}{2} + \sin\left(\beta \frac{3\pi}{2}\right)\right)\right|, = \beta_{min} + (\beta_{max} - \beta_{min}) \times \left(1 - \left(\frac{i}{i_{max}}\right)^3\right)^2 \quad (5)$$

with $\beta_{\min} = 0.2, \beta_{\max} = 1.2$. As the iteration counter i approaches $i_{\max}$, β decreases and ρ_1 contracts, naturally transitioning the LEO from broad exploration to fine-grained exploitation.

GSLEO-AEFA Algorithm

In the initialization, the standard random population generation is done with SRL (Eq. 1) followed by GM (Eq. 2), and the N best candidates are retained. The main loop follows the standard AEFA charge-force-velocity update and then conditionally applies LEO (Eqs. 3-4) to refine each position. The SRL with GM initialization expands the effective sampling radius of the initial swarm; LEO maintains that diversity advantage throughout the search. Together they target AEFA's three failure modes: premature convergence (SRL with GM), exploration exploitation imbalance (LEO's decaying ρ_1), and local optima entrapment (LEO's best-anchored escape branch).

Experiments

Benchmark Functions and Setup

We evaluate GSLEO-AEFA on the 23 -function test suite. F1-F7 are unimodal, F8-F13 are multimoda), and F14-F23 are fixed-dimension. Experiments use 30 independent runs and 1000 iterations at D equal 30, with a fixed population of 30 agents. Six algorithms serve as baselines: AEFA(Anita & Yadav, 2019), PSO (Kennedy & Eberhart, 1995), DE (Storn & Price, 1997), JAYA (Venkata Rao, 2016), SCA(Mirjalili, 2016) , and CS (Yang & Deb, 2010).

Results and Analysis

Table 1 reports the Overall Efficiency (OE). OE is the percentage of functions on which an algorithm records the best mean. GSLEO-AEFA achieves $\mathrm{OE} = 86.95\%$, compared to $CS(39.13\%)$, $\mathrm{DE}(26.08\%)$, and AEFA (21.73%). This dramatic improvement in exploitation precision is attributable to the LEO mechanism, which refines agent positions with a best-anchored perturbation throughout the search. On multimodal functions, GSLEO-AEFA converges to better solutions. Table 2 shows that the proposed GSLEO-AEFA achieved the best Friedman rank, meaning a significant improvement over the compared algorithms.

Table 1. Overall Efficiency of Compared Algorithms

	GSLEO	**AEFA**	**PSO**	**DE**	**JAYA**	**SCA**	**CS**
OE	**86.95%**	21.73%	17.39%	26.08%	4.34%	0%	39.13%

Table 2. Friedman Test Rankings

D	**GSLEO-AEFA**	**AEFA**	**PSO**	**DE**	**JAYA**	**SCA**	**CS**
30	**1.70**	4.74	4.30	3.35	5.07	5.33	3.52

Conclusion

This paper presented GSLEO-AEFA, a physics-inspired global optimizer that extends the Artificial Electric Field Algorithm with two targeted enhancements: a Specular Reflection Learning plus Gaussian Mutation initialization scheme that generates the swarm with broad, asymmetry-free coverage, and a Local Escaping Operator integrated into the per-iteration position update to provide continuous, gradient-free escape from local attractors. Empirical results on 23 benchmark functions demonstrate statistically significant superiority over six state-of-the-art algorithms under Friedman rank. A noted trade-off is that the composite structure-three additional operators layered onto the baseline AEFA-increases per-iteration computational cost. Future work will investigate adaptive operator selection to apply SRL, GM, and LEO selectively based on population state indicators, reducing overhead while preserving diversity benefits. Extension to multi-objective and constrained optimization landscapes represents a natural direction.

References

Adegboye, O. R., & Deniz Ülker, E. (2023). Gaussian Mutation Specular Reflection Learning with Local Escaping Operator Based Artificial Electric Field Algorithm and Its Engineering Application. *Applied Sciences*, *13*(7), 4157. https://doi.org/10.3390/app13074157

Ahmadianfar, I., Bozorg-Haddad, O., & Chu, X. (2020). Gradient-based optimizer: A new metaheuristic optimization algorithm. *Information Sciences*, *540*, 131–159. https://doi.org/10.1016/j.ins.2020.06.037

Anita, & Yadav, A. (2019). AEFA: Artificial electric field algorithm for global optimization. *Swarm and Evolutionary Computation*, *48*, 93–108. https://doi.org/10.1016/j.swevo.2019.03.013

Gandomi, A. H., & Alavi, A. H. (2012). Krill herd: A new bio-inspired optimization algorithm. *Communications in Nonlinear Science and Numerical Simulation*, *17*(12), 4831–4845. https://doi.org/10.1016/j.cnsns.2012.05.010

Heidari, A. A., Mirjalili, S., Faris, H., Aljarah, I., Mafarja, M., & Chen, H. (2019). Harris hawks optimization: Algorithm and applications. *Future Generation Computer Systems*, *97*, 849–872. https://doi.org/10.1016/j.future.2019.02.028

Kaveh, A., & Talatahari, S. (2010). A novel heuristic optimization method: Charged system search. *Acta Mechanica*, *213*(3), 267–289. https://doi.org/10.1007/s00707-009-0270-4

Kennedy, J., & Eberhart, R. (1995). Particle swarm optimization. *Proceedings of ICNN'95 - International Conference on Neural Networks*, *4*, 1942–1948 vol.4. https://doi.org/10.1109/ICNN.1995.488968

Khishe, M. (2023). Greedy opposition-based learning for chimp optimization algorithm. *Artificial Intelligence Review*, *56*(8), 7633–7663. https://doi.org/10.1007/s10462-022-10343-w

Li, S., Chen, H., Wang, M., Heidari, A. A., & Mirjalili, S. (2020). Slime mould algorithm: A new method for stochastic optimization. *Future Generation Computer Systems*, *111*, 300–323. https://doi.org/10.1016/j.future.2020.03.055

Mirjalili, S. (2016). SCA: A Sine Cosine Algorithm for solving optimization problems. *Knowledge-Based Systems*, *96*, 120–133. https://doi.org/10.1016/j.knosys.2015.12.022

Mirjalili, S., Mirjalili, S. M., & Lewis, A. (2014). Grey Wolf Optimizer. *Advances in Engineering Software*, *69*, 46–61. https://doi.org/10.1016/j.advengsoft.2013.12.007

Neri, F., & Cotta, C. (2012). Memetic algorithms and memetic computing optimization: A literature review. *Swarm and Evolutionary Computation*, *2*, 1–14. https://doi.org/10.1016/j.swevo.2011.11.003

Rahnamayan, S., Tizhoosh, H. R., & Salama, M. M. A. (2008). Opposition-Based Differential Evolution. *IEEE Transactions on Evolutionary Computation*, *12*(1), 64–79. https://doi.org/10.1109/TEVC.2007.894200

Rashedi, E., Nezamabadi-pour, H., & Saryazdi, S. (2009). GSA: A Gravitational Search Algorithm. *Information Sciences, Special Section on High Order Fuzzy Sets*, *179*(13), 2232–2248. https://doi.org/10.1016/j.ins.2009.03.004

Singh, A., & Kumar, A. (2021). Applications of nature-inspired meta-heuristic algorithms: A survey. *International Journal of Advanced Intelligence Paradigms*, *20*(3–4), 388–417. https://doi.org/10.1504/IJAIP.2021.119026

Storn, R., & Price, K. (1997). Differential Evolution – A Simple and Efficient Heuristic for global Optimization over Continuous Spaces. *Journal of Global Optimization*, *11*(4), 341–359. https://doi.org/10.1023/A:1008202821328

Venkata Rao, R. (2016). Jaya: A simple and new optimization algorithm for solving constrained and unconstrained optimization problems. *International Journal of Industrial Engineering Computations*, *7*, 19–34. https://doi.org/10.5267/j.ijiec.2015.8.004

Wolpert, D. H., & Macready, W. G. (1997). No free lunch theorems for optimization. *IEEE Transactions on Evolutionary Computation*, *1*(1), 67–82. IEEE Transactions on Evolutionary Computation. https://doi.org/10.1109/4235.585893

Yang, X.-S. (2010). *Nature-Inspired Metaheuristic Algorithms*.

Yang, X.-S., & Deb, S. (2010). *Engineering Optimisation by Cuckoo Search* (arXiv:1005.2908). arXiv. https://doi.org/10.48550/arXiv.1005.2908

Zhang, Y. (2021). Backtracking search algorithm with specular reflection learning for global optimization. *Knowledge-Based Systems*, *212*, 106546. https://doi.org/10.1016/j.knosys.2020.106546